SILVA FENNICA

Silva Fennica 42(5) research articles

www.metla.fi/silvafennica · ISSN 0037-5330
The Finnish Society of Forest Science · The Finnish Forest Research Institute

Appraisal of Seedling Stand Vegetation with Airborne Imagery and Discrete-Return LiDAR – an Exploratory Analysis

Ilkka Korpela, Tuukka Tuomola, Timo Tokola and Bo Dahlin

Korpela, I., Tuomola, T., Tokola, T. & Dahlin, B. 2008. Appraisal of seedling stand vegetation with airborne imagery and discrete-return LiDAR – an exploratory analysis. Silva Fennica 42(5): 753–772.

The potential for combined use of airborne discrete-return LiDAR and digital imagery in the classification and measurement of common seedling stand vegetation was examined in southern Finland (61°50´N, 24°20´E). Classification was based on spectral and textural image features in addition to geometric and radiometric features of the LiDAR. The accuracy of leaf-on, LiDAR-based terrain elevation models was tested as well as the accuracy of LiDAR in the measurement of vegetation heights. LiDAR-based canopy height and the range-normalized intensity of the LiDAR were strong explanatory variables in vegetation classification. Interspecies variation was observed in the height measurement accuracy of LiDAR for different tree, shrub and low vegetation canopies. Elevation models derived with 1–15 pulses per m^2 showed an inherent noise of app. 15–25 cm, which restricts the use of LiDAR in regeneration assessment of very young stands. The spatial pattern of the competing vegetation was reproduced in classification-based raster surfaces, which could be useful in deriving meaningful treatment proposals.

Keywords remote sensing, classification, species, forest regeneration, silviculture
Addresses University of Helsinki, Dept of Forest Management, P.O. Box 27, FI-00014 University of Finland
E-mail ilkka.korpela(at)helsinki.fi
Received 24 June 2008 **Revised** 24 September 2008 **Accepted** 17 November 2008
Available at http://www.metla.fi/silvafennica/full/sf42/sf425753.pdf

1 Introduction

The objectives of forest regeneration and early tending of seedling stands can include optimization of the timber production profitability, consideration of scenic preferences, control of fungal root and foliage disease spread, control of nutrient leaching as well as biodiversity and game management issues (e.g. Piri 2003, Huuskonen and Hynynen 2006, Karjalainen 2006). Forest regeneration and tending of seedling stands involves direct costs. Economically, the investments are

paid back in increased harvesting revenues and a shortened rotation period. The other ecological and social effects may be more difficult to confirm and quantify. The success of a regeneration is assessed some years after planting, sowing or natural regeneration felling, and the result is typically compared with a target stand, which may be defined by a preferred species/size distribution and spatial pattern of crop trees. The future species mixture is controlled by precommercial thinnings and possible complementary planting. An optimal timing of the first precommercial thinning can help in avoiding a costly second precommercial thinning and it affects the economics of the first commercial thinning (Huuskonen and Hynynen 2006). There may be considerable intrastand variation in the stand conditions that, if accurately known, could be utilized for optimization of forest and stand management. The benefits should however pay for the inventory costs.

Remote sensing (RS) of young stands is an attractive option although the emphasis, concluding from the large volume of topical research, has been on the development of methods for the appraisal of mature, commercially important stands. Airborne laser scanning (ALS, LiDAR), especially, is increasingly used in the measurement of timber volume in boreal forests (Næsset 2004, Suvanto et al. 2005). ALS was combined with analysis of aerial images for enhanced results (Maltamo et al. 2006).

Regeneration assessment in managed boreal forests using airborne RS has mostly been concerned with assessment of the density, size, spatial distribution and condition of conifer seedlings using leaf-off very-high resolution imagery (Hall and Aldred 1992, Pouliot et al. 2002, 2005, 2006, Pouliot and King 2005). Hall and Aldred (1992) used visual interpretation of the stocking, density and species in a prestratification and two-stage random sampling setup (Boreal Zone, Saskatchewan, Canada). Photo-plots were assessed at a scale of 1:500 from stereo pairs that were taken using a helicopter-mounted camera. The detection rate of crop trees was dependent on the seedling height, varying from 0% to 94% for height classes between 0–15 cm and 201+ cm. Species identification accuracy between white spruce (*Picea glauca* (Moench) Voss) and jack pine (*Pinus banksiana* Lamb.) was also dependent on the size of the seedling. A scale of 1:5000–1:8000 in which 30-cm-wide crowns would be visible was suggested for the prestratification. Visual interpretation methods tend to be time-consuming and require trained personnel, which has hindered their widespread use. However, the results have provided a basis for the development of automated methods. Pouliot et al. (2005) used semiautomatic tree detection/delineation in 6-cm resolution digital CIR images of 5–10-yr-old planted stands in Ontario (cf. Pouliot et al. 2002, Pouliot and King 2005). The experiment included variation in competing vegetation. The tree detection rates were 48–70% for heights between 0.06 m and 3.0 m. The abundance of competing vegetation also affected tree detection as well as image resolution, parameters of the algorithm and the spatial arrangement of trees.

Competition by other flora was assessed using both manual and automatic interpretation of 2-cm-resolution leaf-off images in Pouliot et al. (2006). Leaf-on large-scale aerial photography was used for identification of general cover types (Pitt and Glover 1993, Pitt et al. 2000) and very-high-resolution digital imagery was tested for cover and leaf-area estimation by Haddow et al. (2000). The requirement for very-high-resolution imagery, valid for both leaf-on and leaf-off, has hindered the adoption of RS in operational regeneration assessment, because the acquisition costs become excessive. Future use of small unmanned aerial vehicles may lead to a reduction in costs. However, in addition to the reduction in data acquisition costs, more reliable and automated analysis methods are needed for the ill-posed task of seedling stand RS.

The potential use of ALS in seedling stands is largely unexplored. Næsset and Bjerknes (2001) examined sparse ALS (1 pulse per m^2) for the estimation of tree height and the stem number in 2–6-m-high stands in Norway. The mean height (H) could be derived from the LiDAR features but the estimates of stand density (S), which is important for treatment proposals, were inaccurate. In Finland, Närhi et al. (2008) tested sparse (0.5 pulses per m^2) ALS for the derivation of treatment need in three classes (no treatment, within 5 years, immediate) in young Norway spruce (*Picea abies* (L.) H. Karst) stands, with H of 2–8 m. The three-class treatment need was not assessed in the

field, but derived later, using estimates of *S* and *H*. Furthermore, regression functions having height-related LiDAR metrics as independent variables were used for the estimation of *H* and *S*. The classification accuracy was 71.8%. RMSEs of *H* and *S* were 16% and 45%, respectively.

Digital, metric multispectral (MS) frame and linear sensors are currently replacing film-based aerial cameras. These new sensors are perceived as well matched for photogrammetric automation due to the improved geometric and radiometric properties of the imagery (Leberl and Gruber 2005). It is feasible to take multiple images of the target and to use this redundancy for enhanced classification and canopy surface reconstruction (Hirschmugl et al. 2007). In forest applications, digital passive sensors are entrusted to improve the species identification task, which is the current bottleneck (Olofsson et al. 2006, Larsen 2007). ALS systems are also evolving with improvements in pulse density, range and orientation accuracy and in the measurement of backscatter reflectance (intensity). Many of the technical problems that were still present in the late 1990s and that resulted in high costs (e.g. accurate sensor orientation, accurate field positioning, elevation modelling and lack of digital workflow; Pitt el al. 2000) now have new solutions (e.g. Korpela 2006, Korpela et al. 2007).

Our aim was to assess the potential of the new data sources, digital MS imagery and discrete-return LiDAR data in the classification and measurement of seedling stand vegetation to support seedling stand management and the derivation of meaningful treatment proposals. For the first time, we tested a newly introduced digital frame camera together with high-density, small-footprint LiDAR in the classification of seedling stand vegetation. To minimize geometric noise in the object-to-sensor mapping and data analysis, we used field samples that were positioned at centimetre-level absolute accuracy. Similarly, image orientation was determined with the utmost precision. The spatial sampling density of the imagery and the LIDAR were higher than what perhaps would be affordable in practice. However, it is justified for exploring the upper limits of accuracy achievable. The spectral image features and features extracted from the LiDAR were tested in the classification of individual plant species and species-classes that could be useful in the derivation of treatment proposals. Our exploratory analysis aimed at basic information and we omitted the variation in image-object-sun geometry (bidirectional reflectance) that affects signals in the images. The thesis is that LiDAR is effective in the estimation of canopy heights. However, in seedling stands the inherent measurement errors may become prominent. Errors in a digital elevation model (DEM) are also directly propagated to canopy height observations. A specific objective was to examine the accuracy of LiDAR-based DEMs in seedling stands and the accuracy of canopy height estimation for common plant species. Typically, the tallest trees in young conifer plantations are deciduous and are removed in precommercial thinnings. We also examined whether the LiDAR-based height observations in combination with image features could be useful in separating the deciduous trees from conifers and other types of vegetation and biotic material. High canopy closure of the broad-leaved trees as measured by LiDAR, would also indicate immediate treatment need. The study confines to artificially regenerated coniferous Scots pine (*Pinus sylvestris* L.) and Norway spruce stands at the ages of 3–13 years.

2 Material and Methods

2.1 Aerial Imagery and LiDAR

The study area is in southern Finland (61°50´N, 24°20´E) near Hyytiälä Forest Station. Leaf-on aerial imagery consisting of 82 exposures was taken with an UltraCAM D digital frame camera from three flight lines (Table 1). Each exposure is a five-channel perspective image that is combined from 13 similar CCD arrays (4000 × 2700, 9-μm pixels) that are almost simultaneously exposed through eight separate lenses equipped with absorption filters. Four subimages constitute an MS image in R, G, B, and NIR that has a lower resolution in comparison to a panchromatic (PAN) image. The sensitivity curves overlap: 390–530 nm (B), 470–660 nm (G), 570–690 nm (R), 670–940 nm (NIR) and 390–690 nm (PAN). The PAN image is fused from nine CCD arrays

that are exposed through four optical cones (Markelin et al. 2005, Honkavaara 2008). We used the level-2, internally preprocessed 16-bit images, in which a small number of defective pixels and rows were corrected by the vendor's processing software.

The exterior orientation of the images was determined using 86 XYZ and 4 Z control points (CPs) and in-flight GPS observations of projection centre positions in a bundle block adjustment. The CPs were treated as error-free and the GPS observations were assigned an a priori accuracy of 0.10 m in the aerial triangulation. Tie points were measured manually and the 765 image observations were assigned an a priori weight of 6 μm. The image residuals of the solution had an RMSE of 5.0 μm. Tables 2 and 3 list the standard deviations of the unknowns. The SDs of the differences in the X, Y and Z coordinates of the CPs were 0.06 m, 0.04 m and 0.16 m, respectively. The inferior accuracy in the Z coordinate is due to the unfavourable base-height ratio of the UltraCAM images.

In a Monte-Carlo simulation with Gaussian image orientation errors, derived using the variance-covariance matrices of the bundle block adjustment, an error-free XYZ point mapped with an average 4-μm error in the PAN image, which corresponds to a half-pixel.

Three leaf-on discrete-return LiDAR (1064 nm) datasets from 2004, 2006 and 2007 were used (Table 4). Acquisition in 2006 occurred 1 week prior to the aerial photography and 4 weeks before the fieldwork. The LiDAR of 2006 was used for vegetation mapping and terrain modelling was tested using all LiDAR datasets.

The geometric accuracy and relative matching of the image and LiDAR data sets were assessed by superimposing LiDAR points in the aerial images and by using surfaces and borders for which the XYZ coordinates were measured using Network RTK (Wanninger 2005) satellite positioning. The XY accuracy of the LiDAR datasets was 0.25 m or better. The Z accuracy was better than 0.1 m. The point densities showed considerable spatial variation, due to the scanning geometry (Fig. 1).

Table 1. Characteristics of the aerial imagery.

Camera	Vexcel UltraCAM D
Date	August 2, 2006
Time, UTC	06:20–06:40
Solar elevation	29.6°
Resolution, Panchromatic (PAN)	7500 × 11 500 pixels, 0.09 m
Resolution, Multi-spectral (MS)	2400 × 3680 pixels, 0.27 m
Focal length, PAN/MS	105.2 mm / 35 mm
Dynamic range, nominal	14 bits
Image overlaps, forward / side	60% / 30%
Aperture, shutter speed	F8, 1/175 s
Base/height ratio	260 m / 1000 m
Image coverage	670 m × 1035 m

Table 3. Standard deviations of 169 tie point coordinates [m].

	X	Y	Z
Mean	0.08	0.05	0.23
Min	0.03	0.03	0.07
Max	0.27	0.13	0.54

Table 2. Standard deviations of the exterior orientation parameters, [rad] and [m].

	Attitude parameters			Projection centre coordinates		
	ω	φ	κ	X_0	Y_0	Z_0
Mean	0.000094	0.000088	0.000077	0.09	0.10	0.06
Min	0.000087	0.000078	0.000044	0.09	0.09	0.04
Max	0.000106	0.000098	0.000158	0.10	0.10	0.14

Table 4. Characteristics of the LiDAR datasets.

Instrument	ALTM2033	ALTM3100	ALS50-II
Date	August 5, 2004	July 25, 2006	July 4, 2007
Time, UTC	13:00–13:30	15:41–16:57	15:40–17:20
Flying speed	~75 m/s	~75 m/s	~66 m/s
Pulse/scan freq.	33.3 kHz / 29 Hz	100 kHz / 70 Hz	115.8 kHz / 52 Hz
Point density	0.7–2 / m^2	6–9 / m^2	7–12 / m^2
Footprint diameter	25–29 cm	25–28 cm	17–18 cm
Strips per point	1–2, 20% overlap	2–3, 55%	2–3, 55 %
Scan angle	± 20°	± 14°	± 15°
Range, m	860–960	810–890	750–850
Returns	1 or 2	1, 2, 3 or 4	1, 2, 3 or 4
Range discrimination distance	4.5 m	3 m	3.5 m
Intensity	8 bits	12 bits	8 bits, returns 1–3

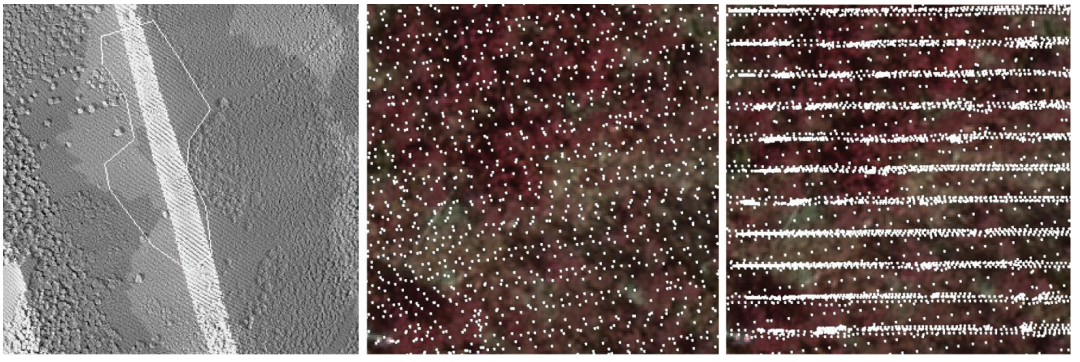

DENSITY 2006 & 2007 2006 2007

Fig. 1. Left: a 300 × 300-m map of LiDAR point density in seedling stand 6. The greyscale denotes density, 6–29 first-return points per m^2 for the combined data of 2006 and 2007. Middle and right: 17 × 17-m aerial views from the high-density area show the point patterns of the 2006 and 2007 data, respectively.

2.2 Observations of Vegetation Field Samples

The field data were collected in August, 2006 in six seedling stands, where moraine soils prevailed and soil preparation by mounding or harrowing was applied (Table 5, Fig. 2). Two sampling schemes were used. First, each stand was sampled along lines with an entire coverage. These 947 samples were selected at approximately equidistant locations and represented homogenous samples of the 27 targets listed in Table 6. A second sampling included all trees and shrubs (n = 645) inside square-shaped plots that were subjectively located to include variation in stand conditions. All samples were positioned and measured for height and species. Network RTK positioning, which has an accuracy of 3–5 cm in XYZ, was used (Häkli 2004, Wanninger 2005). The sample height was measured in 0.1-m nominal accuracy, using a reference pole (Fig. 3).

Altogether 27 classes were defined, which were further divided into four operational classes (OCs) that were considered important for the derivation of meaningful treatment proposals in coniferous seedling stands (Table 6). The OCs comprised 1) coniferous trees, 2) broad-leaved trees for potential removal, 3) low vegetation and 4) abiotic material.

1: Planted spruce

2: Planted spruce

3: Sowed pine and planted spruce

4: Planted spruce

5: Planted spruce

6: Planted pine

Fig. 2. Photographs of stands 1–6 in August 2006 during the fieldwork.

Table 5. Stand information in 2006.

Stand	Age	Area, ha	Lines	Plots				All observations	
			N_{obs}, lines	N_{obs}, plot	Area, m^2	Trees, n/ha	Mean h, m	Mean *h*, m conifers	Mean *h*, m broad-leaved
1	8	1.83	138	119	225	5289	1.33	0.9	1.6
2	7	0.69	224	74	100	7400	2.70	2.2	2.7
3	13	1.52	151	112	100	11200	2.75	2.9	3.2
4	5	1.97	146	88	150	5867	1.40	1.1	1.7
5	3	0.57	139	160	150	10067	1.30	1.2	1.5
6	10	1.09	149	92	225	4089	1.62	2.3	1.7

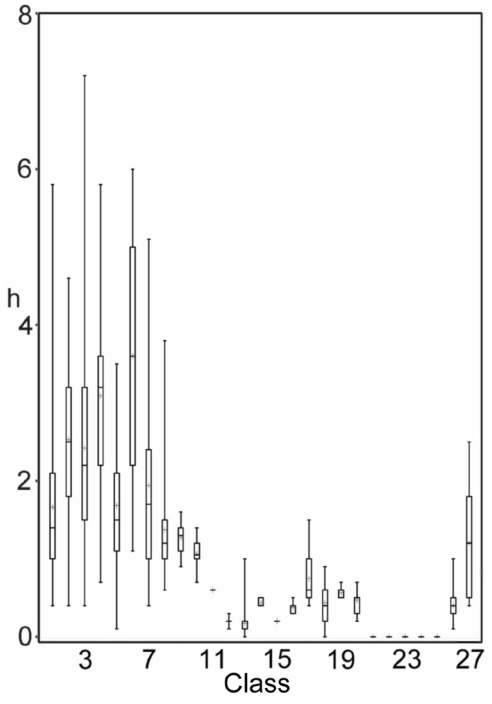

Fig. 3. Box-whisker plot of vegetation heights in the 27 target classes (Table 6). The box is drawn from the 25th to the 75th percentile and the height range is marked by the line.

2.3 Feature Extraction

2.3.1 Image Features

As a result of the imaging geometry (diagonal field-of-view 60°) and solar angles (zenith ~60°, azimuth ~108°), the phase-angles ranged from 33° to 89°. Bidirectional reflectance effects were thus present in the images and undoubtedly affected the spectral values observed. Fig. 4 illustrates the effect for Scots pine and Norway spruce seedlings. Shadowed targets also prevailed in the images, due to the low solar elevation.

In all, the field observations mapped to 21 images and 5467 image points. The extraction of nine image features was performed with an in-house photogrammetric workstation. The *R*, *G*, *B* and *NIR* values of the nearest pixel formed the pixel-level spectral features in 27-cm resolution as well as the normalized difference vegetation index, *NDVI*:

$$NDVI = \frac{(NIR - R)}{(NIR + R)} \quad (1)$$

The *NDVI* separated vegetation effectively in the shaded areas, probably due to the high dynamic range of the images. The textural features PAN_{Mean}, PAN_{SD}, PAN_{Min} and PAN_{Max} were calculated from 3×3 pixel windows of the 9-cm resolution PAN image.

To enable shadow masking and analysis of the effects of shadowing, the first author measured the training data – XYZ points in shadow and direct light (424 + 410), using manual least-square ray-intersection of the aerial images. Random selection of points in all stands was pursued. Image features were extracted for these points and Fisher's linear discriminant analysis (LDA) was applied for the binary classification. The classification accuracy was 96% with *NIR*, *NDVI*, *G*, *R* and *B* (Fig. 5). The errors were mainly due to misclassifications in the training data. Namely, a portion of the points that mapped to more than two or three images, i.e. to additional oblique views, were occluded by other (higher) targets.

Mapping of the field observation to the nearest image pixel was examined by systematically

Table 6. The 27 target types classified in the field and their division into four operational classes (OCs). R is the rank by occurrence frequency of understorey species on mineral forest soils in Finland. Similarly, F is the average frequency of occurrence and D the average coverage in stands less than 20 yr old according to Hotanen et al. (2000).

	Woody plants		Number of observations			Hotanen et al. (2000)		
		OC	Lines	Plots	All	R	F, %	D, %
1	*Picea abies*	1	118	129	247	–	–	–
2	*Pinus sylvestris*	1	79	33	112	–	–	–
3	*Betula.*	2	163	255	418	–	–	–
4	*Populus tremula*	2	30	29	59	–	–	–
5	*Sorbus aucuparia*	2	90	157	247	–	–	–
6	*Alnus incana*	2	15	0	15	–	–	–
7	*Salix*	2	60	38	98	–	–	–
8	*Juniperus communis*	2	29	4	33	–	–	–
LOW VEGETATION								
9	*Chamerion angustifolium*	3	24	–	24	18	38	1.7
10	*Rubus idaeus*	3	49	–	49	44	10.5	1.0
11	*Pteridium aquilinum*	3	1	–	1	81	2.6	0.5
12	*Vaccinium myrtillus*	3	4	–	4	3	65	3.5
13	*Vaccinium vitis-idaea*	3	28	–	28	2	86	5.0
14	*Vaccinium uliginosum*	3	3	–	3	19	–	–
15	*Empetrum nigrum*	3	1	–	1	12	25	2.0
16	*Calluna vulgaris*	3	21	–	21	20	25	4.4
17	*Calamagrostis epigejos*	3	70	–	70	64	5.0	0.7
18	*Deschampsia flexuosa*	3	59	–	59	4	68	11
19	*Luzula pilosa*	3	4	–	4	13	37	0.5
20	*Carex*	3	13	–	13	–	–	–
21	*Pleurozium schreberi*	3	4	–	4	1	74	21
22	*Hylocomium splendens*	3	2	–	2	6	27	1.6
23	*Cladina/Cladonia*	3	8	–	8	–/5	31/32	3.9/0.7
ABIOTIC TARGETS								
24	Mineral soil surface	4	5	–	5	–	–	–
25	Stone/rock surface	4	30	–	30	–	–	–
26	Logging residue	4	29	–	29	–	–	–
27	Dry wood surface	4	8	–	8	–	–	–
TOTAL			947	645	1592			

lowering the vegetation sample. We hypothesized that this would result in better positioning of the image features in non-nadir views, since the pixels would capture more of the object. The shift downwards was proportional to the object height: $\Delta Z = -\ h \times (1 - lc)$. Parameter *lc* was assigned values between 0 and 0.35 in steps of 0.05 and the image features were stored for analysis. The number of observations classified as being in direct light was maximal when *lc* was 0.25, which was later applied for trees, i.e. classes 1–9. The image features were highly correlated, except for the NIR band (Table 7).

2.3.2 LiDAR Features

Three LiDAR features were extracted for each field observation, using the first-return points of the 2006 ALTM3100 data:

- Proportion of ground returns, *PGR*
- LiDAR-based height above ground, h_{LiDAR}
- Intensity of the nearest pulse, INT_{norm}.

We hypothesized that *PGR* measures canopy closure and leaf density. It may be used to separate dense broad-leaved species from coniferous canopies and tall grasses. h_{LiDAR} is the height of the nearest LiDAR return. The height growth

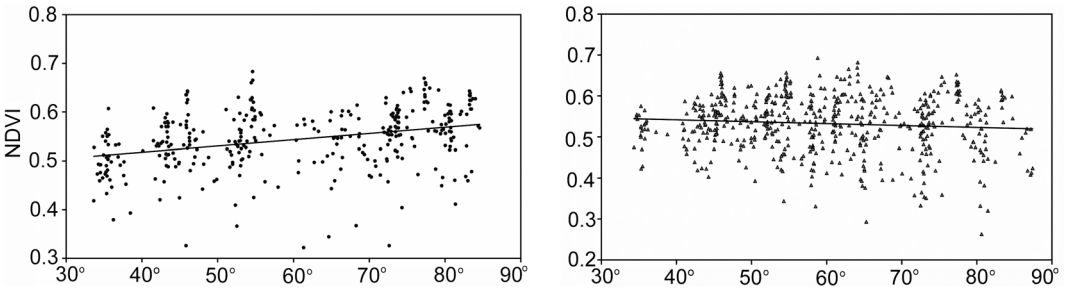

Fig. 4. *NDVI* phase-angle scatterplots for pine (left) and spruce (right). The phase-angle is the angle between the object-to-camera and object-to-sun 3D vectors.

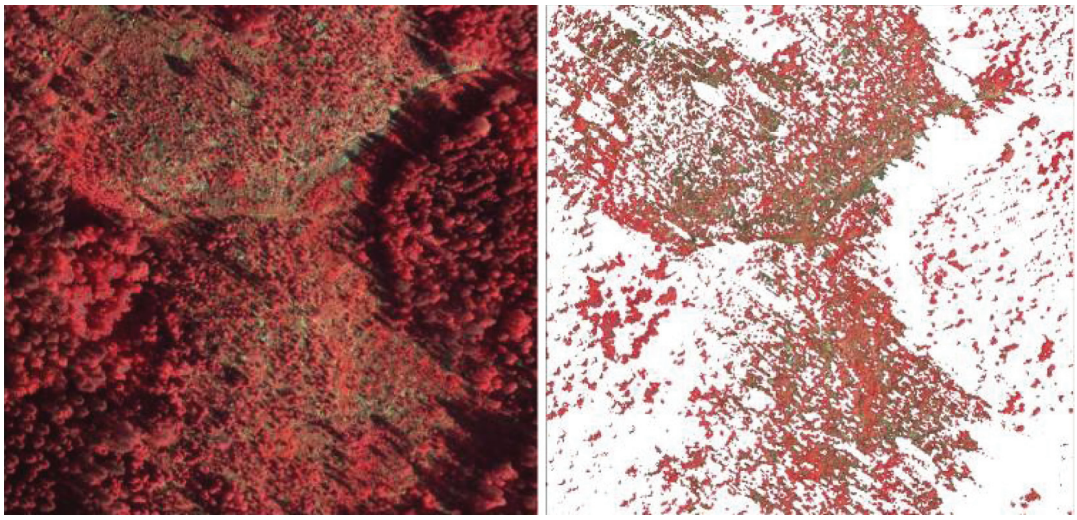

Fig. 5. Example of a 150 × 150-m false-colour aerial image of stand 6 and the corresponding shadow classification, in which the shaded pixels are in white.

Table 7. Pearson correlation coefficients of image features. All 5467 observations.

	R	*G*	*B*	*NIR*	*NDVI*	PAN_{Mean}	PAN_{SD}	PAN_{Max}	PAN_{Min}
R	1	0.95	0.94	0.46	–0.63	0.93	0.59	0.91	0.89
G		1	0.92	0.61	–0.44	0.95	0.56	0.92	0.92
B			1	0.33	–0.62	0.92	0.58	0.91	0.88
NIR				1	0.31	0.49	0.23	0.46	0.49
NDVI					1	–0.51	–0.44	–0.54	–0.45
PAN_{Mean}						1	0.61	0.97	0.96
PAN_{SD}							1	0.76	0.37
PAN_{Max}								1	0.88
PAN_{Min}									1

Table 8. Pearson correlation coefficients of LiDAR features. All 1592 observations.

	PGR	h_{LiDAR1}	INT_{norm}
PGR	1	–0.68	0.18
h_{LiDAR}		1	–0.41
INT_{norm}			1

rhythm of coniferous seedlings differs from that of broad-leaved trees. Given the stand age and predicted heights, h_{LiDAR} possibly separates the fast-growing and thus taller broadleaved species from the conifers. LiDAR intensity is a quantity analogous to backscatter reflectance in optical data. Unlike images, LiDAR is insensitive to shadows. The geometry and density of the foliage encountered by the LiDAR beam are likely to affect the measured backscatter. INT_{raw} is the recorded intensity and INT_{norm} is normalized for the variation in the scanning range, which exercises a considerable effect (e.g. Korpela 2008).

PGR was calculated from points inside a 0.5-m radius. The ground elevation was taken from accurate GPS field measurements. LiDAR points that deviated < 0.5 m from Z_{ground} were considered as ground returns; h_{LiDAR1} was the height of nearest LiDAR point. The intensity of the nearest LiDAR point was normalized for the variation in scanning range:

$$INT_{norm} = (R / R_{ref})^{a} \times INT_{raw} \quad (2)$$

In Eq. 2, a was 2.5. Theoretically, $a = 2$ for homogenous surfaces larger than the LiDAR footprint, $a = 3$ for linear objects and $a = 4$ for individual large scatterers (Ahokas et al. 2006, Kaasalainen et al. 2007). The value 2.5 is a compromise that was determined using artificial surfaces and natural targets, including understorey shrub, lichen and moss vegetation (Korpela, 2008). R_{ref} in Eq. 2 is an average reference range, which was 839 m.

The highest INT_{norm} values were observed for *R. idaeus* (raspberry, class 10 in Fig. 6). *P. sylvestris* (class 2) had a lower average LiDAR intensity than *P. abies* (1), but it may have resulted from mixing with other low vegetation because the *P. abies* seedlings were rather short. *S. aucuparia* (5) had a clearly higher intensity than *Betula* (3), which did not separate from *P. abies* (1) or *P. tremula* (4) (Fig. 6.).

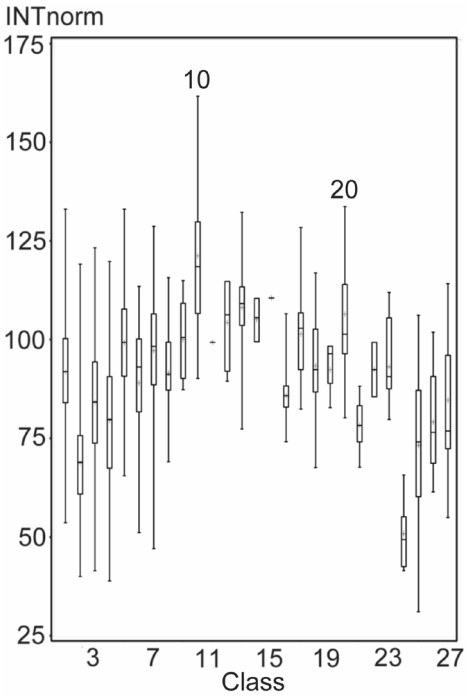

Fig. 6. Box-whisker plot of INT_{norm} for target classes 1–27 (Table 6). The box is from the 25th to the 75th percentile and the range is depicted by the line.

2.4 Linear Discriminant Analysis for Object Classification

The Stepdisc and Discrim discriminant analysis procedures in SAS/STAT (SAS Institute Inc., Cary, NC, USA) statistical software (version 9.1.3) were used for feature selection, classification and leave-one-out type of cross-validation. Stepdisc performs a stepwise feature selection and Discrim was later used for LDA.

The classification performance was measured with the proportion of correctly classified objects and the simple kappa (Cohen 1960):

$$\kappa = \frac{P(A) - P(E)}{1 - P(E)} \quad (3)$$

In Eq. 3, $P(A)$ is the proportion of correctly classified objects and $P(E)$ the expected proportion from random classification.

In LDA, it is assumed that the multivariate within-class distributions are approximately

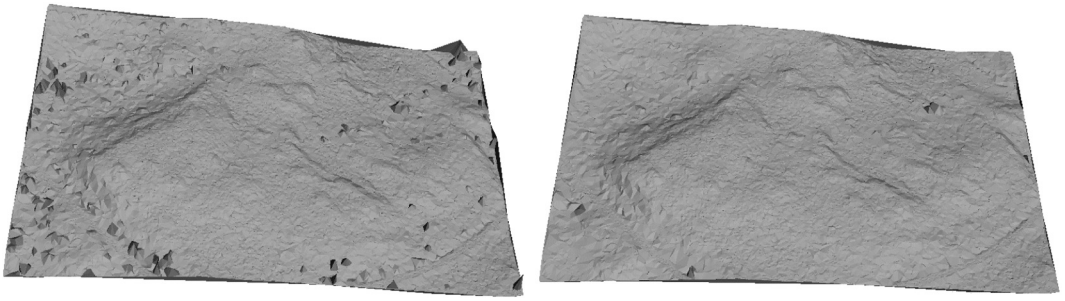

Fig. 7. Visualization of the nonfiltered and filtered D-TIN of seedling stand 1 over an area of 300 m × 200 m.

normal. Multivariate normality (MVN) was tested using Mardia's skewness and kurtosis tests as well as the Henze-Zirkler's test. The data did not fulfil all of the MVN assumptions, mainly because of the skewness of the distributions. The data was assumed to be outlier-free making LDA applicable.

2.5 Terrain Modelling

TerraModeler by Terrasolid (Jyväskylä, Finland) was used for processing the 2004 LiDAR data into a 1-m raster DEM, referred to as 2004-Terra. TerraModeler is based on three principal parameters (Axelsson, 2000) that were tried in 100 combinations and a best-case DEM with an RMSE of 0.27 m was selected for the tests here. The RMSE was observed in 8329 reference height points in mature forests across the same study area (Korpela and Välimäki, 2007).

An in-house DEM algorithm was applied for testing the effect of LiDAR point density on DEM accuracy, using all LiDAR datasets. The area in the algorithm flow is first divided into a raster, according to the parameter *CellSize*. The point with minimum Z is sought in each cell and all points that deviate less than the value of parameter *Zbuffer* from this minimum are stored for D-TIN estimation (Delaunay – Triangulated Irregular Network). This TIN is iteratively filtered for rising outlier peaks by removing nodes that can only 'be reached' by steep triangle facets. A threshold parameter, *SlopeThreshold* at 15°, was applied. The filtering is continued typically in 3–4 iterations, until the visual appearance is satisfactory (Fig. 7). Finally, the TIN is converted into a 1-m resolution raster model. This conversion introduces a small random error of 0.03–0.07 m. The TIN-estimation was done with fast, streaming algorithms by Isenburg et al. (2006).

The DEM algorithm is not optimal, because it results in higher point densities in planar nonvegetated areas and is somewhat limited in capturing fine topographic details. The parameter *CellSize* should be minimized to reproduce the details. However, the reduction in *CellSize* also reduces the probability that the lowest point in a cell is a true ground observation, which may lead to bias. If parameter *Zbuffer* is set to a very high value, it causes the DEM to float above the true ground.

2.6 Raster Analysis of the Canopy Layer

To determine how the sensor fusion and object classification could be applied in practice, we carried out a raster analysis, in which the fully mapped plots were classified in a 0.5-m grid. LiDAR features at each grid point were computed such that the *PGR* was estimated inside a 1-m-wide circle and h_{LiDAR} and INT_{norm} inside a 0.7-m-wide square, using the highest LiDAR point. The image features were derived by mapping the highest LiDAR point to the image with the smallest off-nadir angle. The OC was determined, using LDA functions derived from eight image and LiDAR features and the training data of the particular stand. A reference grid was calculated, using the reference trees; in it, the OC was determined by the tallest tree in each grid cell.

Table 9. Accuracy of the elevation models, n = 1592.

DEM	Points/m^2	Mean	SD	RMS	Min	Max
2004-Terra	0.7–1.4	–0.08	0.21	0.22	–0.91	+1.22
2004	0.7–1.4	–0.13	0.26	0.30	–1.70	+1.31
2006	6–9	–0.21	0.19	0.28	–1.65	+1.28
2007	7–10	–0.12	0.19	0.22	–1.93	+1.43
2006&2007	12–16	–0.14	0.18	0.23	–1.17	+1.38

3 Results

3.1 Accuracy of Leaf-on LiDAR-based Elevation Models

In all, five DEMs were compared and were all above the reference ground (Table 9). The in-house DEM algorithm was inferior in comparison to the performance of the TerraModeler algorithm with the same 2004 LiDAR data. Increase in point density from 1 to 15 per m^2 lowered the RMSE 36%, from 0.30 m to 0.22 m.

The errors of the different DEMs were correlated (Table 10). We suggest that 36–64% of the random error variance could have been due to the properties of the reference data. The errors may also have been correlated due to the estimation method, since the same XY grid and values of parameter *Zbuffer* were applied in each stand. Part of the observed random error may also have been due to errors in the reference measurements made with Network RTK. In addition, the subjective selection of the line samples and penetration of the GPS antenna rod into the soil may have been sources of systematic errors in the reference data. However, the low vegetation probably reduced the number of true ground returns, thus lifting the DEMs upwards; while a considerable portion of the random errors were probably due to the small-scale variation in the relief, which cannot be captured by the DEMs. This inherent random error was 0.15–0.25 m and suggests that very low canopies cannot be reliably measured using LiDAR, because this inherent DEM noise propagates directly to the height estimates.

There may also have been small XY or Z offsets at the project and strip levels in the LiDAR datasets. It is evident that changes in low vegetation have occurred between 2004 and 2007 (vegetation succession), which suggests that the results are most reliable for the 2006 DEM, the year of fieldwork. The errors were largest in stand 3, which has a dense 3–5-m-high canopy of sowed, planted and naturally regenerated trees on rather fertile soil that was harrowed in 1994.

Table 10. Correlation coefficients of the residuals of the five DEMs, n = 1592.

DEM	2004-Terra	2004	2006	2007	2006&2007
2004-Terra	1				
2004	0.63	1			
2006	0.67	0.70	1		
2007	0.60	0.63	0.87	1	
2006&2007	0.64	0.69	0.90	0.91	1

3.2 Accuracy of LiDAR-based Canopy Heights

The use of h_{LiDAR} resulted in underestimation of tree heights of from 19% to 39% or 0.54–1.09 m (Table 11). The coefficients of variation (CVs) ranged from 17% to 37%. The height of the relatively large-leaved raspberry (*R. idaeus*) was underestimated by 29% but the precision was rather high, 13% in CV. Rosebay willowherb (*C. angustifolium*), which has a comparable mean height but a different leaf structure, was underestimated by 52% (CV = 13%). The results which are biased and rather noisy imply that the vegetation height measurement accuracy of LiDAR is restricted and dependent on the species.

Table 11. Accuracy of h_{LiDAR} excluding DEM errors. Classes with over 30 observations were included.

Class	N	Mean h, m	Mean Δh, m	h_{LiDAR}, %	CV, %
1 Spruce	854	1.66	+0.65	61	37
2 Pine	450	2.53	+0.77	69	21
3 Birch	1314	2.42	+0.84	65	23
4 Aspen	152	3.09	+1.09	65	30
5 Rowan	900	1.69	+0.54	68	28
6 Alder	66	3.60	+0.69	81	17
7 Willows	332	1.94	+0.73	63	29
8 Juniper	103	1.37	+0.48	65	27
9 Rosebay willowherb	99	1.28	+0.67	48	13
10 Raspberry	170	1.07	+0.31	71	14
13 Lingonberry	98	0.17	–0.05	128	122
16 Heather	69	0.38	+0.12	67	24
17 Small-reed	256	0.75	+0.43	43	32
18 Wavy hair-grass	192	0.44	+0.25	42	48
20 Sedges	46	0.47	+0.27	43	22
23 Reindeer lichens	38	0.00	–0.10	–	–
24 Mineral soil	30	0.00	–0.14	–	–
25 Stone / rock	111	0.00	–0.06	–	–
26 Logging residues	107	0.40	+0.06	84	37
27 Dry round wood	28	1.21	+0.64	47	57

3.3 Vegetation Classification Using LiDAR and Image Features

LDA was first applied in each stand for classifying the four operational target types (Table 12). The classification accuracy varied from 61.1% to 78.9% and was reduced if the shadowed targets were included (Table 13). *NDVI* and INT_{norm} were strong features. Similarly, h_{LiDAR1} was significant in stands 1–4, in which the height of the broad-leaved trees differed from that of the conifers.

The best accuracy, 77.8% for the OCs was achieved in stand 6. The confusion matrix of this classification is given in Table 14.

The classification accuracy for all 27 classes using 3787 sunlit observations from all six stands, was 39% ($\kappa = 0.28$) with eight image and LiDAR features. With image and LiDAR features only, the accuracy fell to 28% ($\kappa = 0.19$) and 24% ($\kappa = 0.15$), respectively.

3.4 Raster Analysis

The raster analysis is illustrated in Figs. 8–10. Since the 0.49-m^2 raster cells had overlaps in the 0.5-m raster and since the reference raster was computed using the stem positions, comparison of the two surfaces was not straightforward. The reliability of operational class 2 (the competing trees) was considered essential. Those parts of a conifer seedling stand that have a dense dominant canopy cover of broad-leaved trees are likely in need of immediate clearing. In stand 1, the classification accuracy was low and the classified grid overestimates the portion of conifers and partly fails in accurate determination of the broad-leaved canopy (Fig. 9).

The spatial structure of the canopy of the broad-leaved trees was reproduced by the classifications in stands 2–4 (Fig. 10). Based on the results, we suggest that further processing of the classified raster surfaces (e.g. segmentation) will enable derivation of maps of intrastand treatment proposals.

Table 12. Classification results for the four operational classes: conifers, competing broad-leaved trees, low vegetation and abiotic material. Observations in direct light only.

Stand	κ	N	% correct	Features, max 8
1	0.44	639	61.6	$R\ G\ B\ IR\ NDVI\ PAN_{SD}\ h_{LiDAR1}\ INT_{norm}$
2	0.47	383	74.6	$R\ G\ B\ PAN_{SD}\ h_{LiDAR1}\ PGR\ INT_{norm}$
3	0.45	611	68.2	$R\ G\ IR\ NDVI\ h_{LiDAR1}\ PGR\ INT_{norm}$
4	0.57	727	70.7	$R\ G\ B\ NDVI\ PAN_{Mean}\ h_{LiDAR1}\ PGR\ INT_{norm}$
5	0.59	392	71.4	$R\ G\ B\ IR\ NDVI\ PAN_{Max}\ PGR\ INT_{norm}$
6	0.69	1035	78.9	$R\ G\ B\ IR\ NDVI\ PAN_{SD}\ PGR\ INT_{norm}$

Table 13. Classification results for the operational classes: conifers, competing broad-leaved trees, low vegetation and abiotic material. All observations.

Stand	κ	N	% correct	Features, max 8
1	0.44	729	61.1	$R\ G\ B\ IR\ NDVI\ PAN_{SD}\ INT_{norm}\ h_{LiDAR1}$
2	0.49	694	69.7	$R\ IR\ NDVI\ PAN_{Mean}\ PAN_{Max}\ PGR\ INT_{norm}\ h_{LiDAR1}$
3	0.47	1166	65.3	$R\ G\ IR\ NDVI\ PAN_{Max}\ PGR\ INT_{norm}\ h_{LiDAR1}$
4	0.57	833	70.8	$R\ G\ B\ IR\ NDVI\ PAN_{Max}\ INT_{norm}\ h_{LiDAR1}$
5	0.44	808	62.0	$R\ G\ B\ IR\ NDVI\ PAN_{SD}\ PGR\ INT_{norm}$
6	0.67	1237	77.8	$R\ G\ B\ IR\ NDVI\ PAN_{SD}\ PGR\ INT_{norm}$

Table 14. Error matrix (%) of best-case LDA classification in stand 6. Objects in shadow and direct light.

Class	N	Classified into, %			
		1	2	3	4
1 Conifer	339	80.2	14.5	5.3	0.0
2 Broad-leaved	486	17.1	72.2	10.7	0.0
3 Low vegetation	122	0.8	9.0	89.3	0.8
4 Abiotic material	88	2.3	0.0	1.1	96.6

4 Discussion of Results and Conclusions

RS is an attractive option for the assessment of young seedling stands. Recent advances in sensor technology allow for detailed and geometrically accurate analysis and sensor fusion of optical and active data in 3D object classification, which was tested here for the first time in seedling stands. The experimental setup was limited; i.e. it did not include wide variation in stand conditions or topography, one image scale and camera were used and only one set of LiDAR data was tested. In addition, separate training and validation datasets were not used for the classifications. These factors affected the interpretation of the results and were accounted for. The geometric orientation of the field samples and the sensors was also established with the utmost precision. This provided a solid basis for the analysis.

We hypothesized that being able to measure canopy heights is crucial, since the growth rhythm of conifer seedlings and the pioneering broad-leaved trees differs, thus enabling their separation. LiDAR produced DEMs that were 8–20 cm above the true ground. These results are in line with earlier findings (Korpela and Välimäki 2007). The random error was app. 0.2 m and the increase in point density from 1 to 15 points per m^2 reduced noise only marginally. DEM errors apparently cause an inherent inaccuracy of app. 0.25 m in plant/canopy height estimates. The noise can be higher under very dense canopies, where the probability of LiDAR registering true ground is lower, or under more complex topographic conditions.

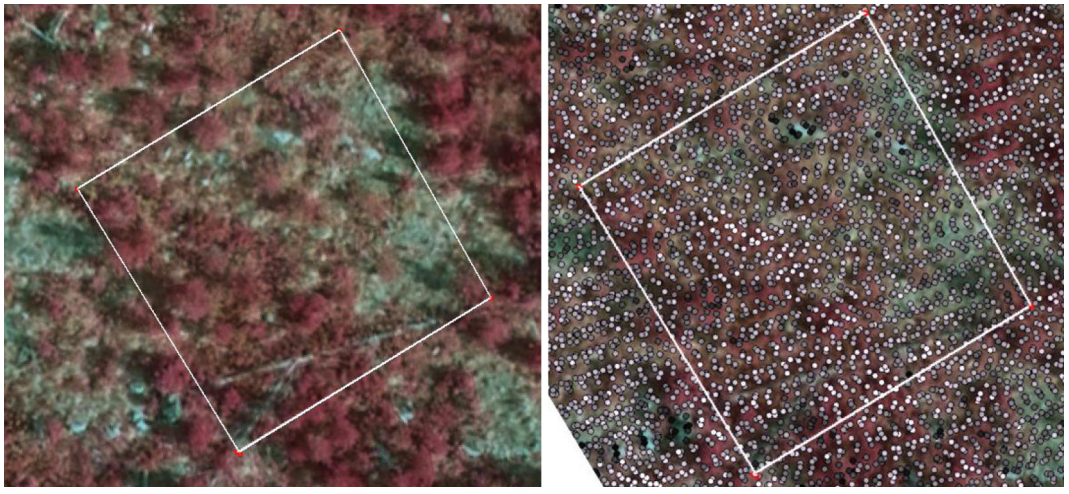

Fig. 8. The 225-m^2 plot in stand 1 seen in a near-nadir false-colour image. The plot had 26 spruce seedlings (1155 s/ha, H = 0.70 m), 44 birches (1955 s / ha, H = 1.72 m) and 47 rowans (2088 s/ha, H = 1.34 m). The LiDAR points are superimposed in the view on the right and the circular greyscale denotes intensity, $INT_{norm} \in [46,132]$.

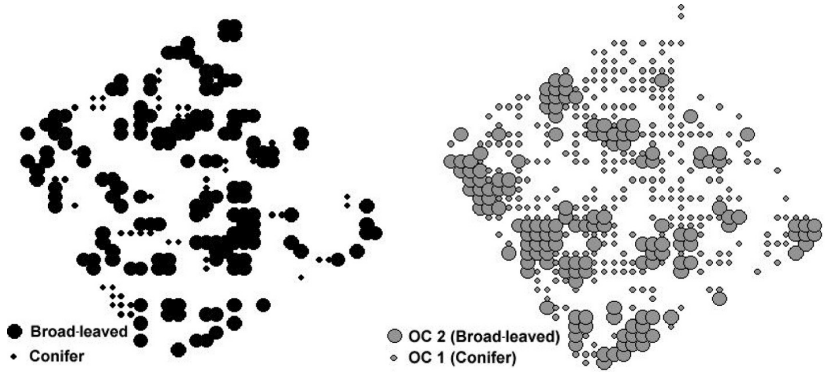

Fig. 9. Left: reference grid of operational classes derived from the field-measured trees. Right: Classification using eight image and LiDAR features (cf. Table 13). Stand 1.

Due to the random errors in terrain elevation and canopy heights, we feel that airborne LiDAR is not applicable in very young seedling stands. We suggest that multi-image matching (Hirschmugl et al. 2007) may be used to enhance the accuracy of canopy height (surface model).

The potential for use of semi-dense, small-footprint LiDAR (6–9 p/m^2, 0.3 m) in estimating the top elevation of individual plants and plant canopies in seedling stands was limited. Underestimation of heights was observed, which was dependent on the species. This complicates sensor fusion, because the LiDAR reflection point that is mapped to the images for the retrieval of image features is not necessarily from the outer, photovisible canopy; in addition the images and LiDAR view the targets in different geometries. The underestimation of tree heights varied from 20% to 40% with a CV of app. 30%. The relative height difference of the conifer seedlings and the broad-leaved species, birch and aspen especially, can be 100% in seedling stands because of the differences in juvenile growth (e.g. Elfving 1982, Miina and Saksa 2008). If models are available

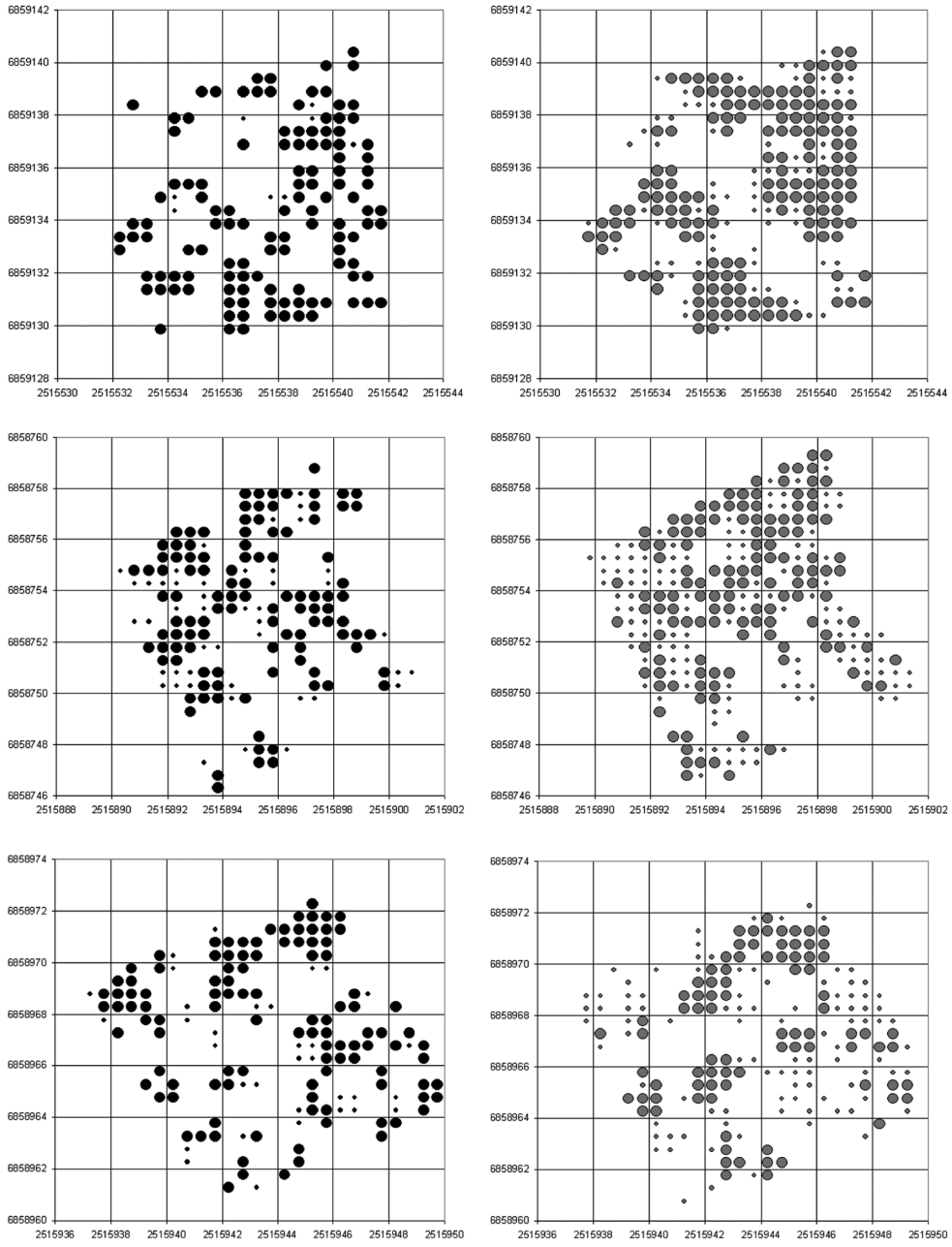

Fig. 10. Reference (left) and classified (right) grids of broad-leaved (●) and conifer (·) vegetation in the 100-m^2 plots of stands 2 (upper), 3 (middle), and 4 (lower). Classification was carried out, using eight image and LiDAR features (cf. Table 13).

for the prediction of juvenile height growth of trees, the model estimates can be used in the LDA classification of seedling stand targets, using the expectances and variances of heights and an empirical covariance structure of the other discriminant features. Naturally, the height estimates need to be unbiased or otherwise the classification will fail. The height growth difference of sprouting broad-leaved stools vs. trees regenerating from seed further complicates the use of LiDAR-based heights in classification.

The 27 classes consisting of common tree species, shrubs, grasses, mosses and other surface types that typically occur in seedling stands could not be reliably classified using the tested image and LiDAR features. For the 27 classes, the overall classification accuracy was 39%. In the stand-level tests, the classification accuracy varied from 61% to 79% for the four operational classes of conifers, broad-leaved trees, other low vegetation and abiotic surfaces. These classes were considered sufficient for the determination of meaningful treatment proposals and stand projections. This rather high level of accuracy was attained with considerable training data. The raster analysis revealed that the spatial pattern of the broad-leaved trees is potentially retrievable, using sensor fusion and classification with image and LiDAR features. Further work with more representative field material (stand types, time of season) and different RS material (image scales, sensor types, sampling density) is required for the development of practical applications. For example, we suggest testing of the ADS40 multiview line sensor (Leica Geosystems, Norcross, GA, USA) because its colour registration (beamsplitter) differs from those in metric digital frame cameras (absorption filter). In general, digital cameras offer means of using redundancy for enhanced classification results and we suggest method development in multiview classification. This requires that the object classification occurs in 3D, which is easier to implement using LiDAR with images than by images alone (Hirschmugl et al. 2007). In addition, we suggest investigating the use of more complex image and LiDAR features for vegetation classification.

Range-normalized intensity of LiDAR was a strong explanatory variable in seedling stand vegetation classification. It is invariant to target location, unlike the image features used. Unfortunately, the intensity did not separate the three main species of forest trees in Finland. LiDAR-based height was usable in stands, where the conifers were shorter than the broad-leaved trees. The spectral image features were not compensated for the varying image-object-sun geometry even though the spectral values varied with the imaging geometry and that the effect varied between species. This is explained by the varying bidirectional reflectance distribution (BRD) of different targets. Further work is needed to study these directional effects and their compensation, or preferably, utilization in an image-based species classification task. We thus suggest that BRD research be initiated to quantify these BRD effects and to separate them from biological noise (tree vigour, diseases, leaf density, epiphytic lichens etc.) and trends (tree size/age). Such basic research could also aid in constructing specific sensors (radiometric properties) for forest vegetation mapping. Currently, cameras and LiDAR sensors are mainly built for topographic mapping and are commonly used by foresters.

Traditional satellite image-based change detection procedures can be applied for estimating the proportion of deciduous trees in large regeneration stands (Häme 1991) or when existing stand database information supports the interpretation (Varjo 1997). The presence of small-scale structural variation, small size of regeneration areas and the lack of multitemporal data lead to the conclusion that the resolution of traditional (e.g. Landsat) imagery is not sufficient for reliable regeneration monitoring in Finland (Häme et al. 1998, Saksa et al. 2003, Pesonen et al. 2007). Instead of applying the new very-high-resolution (< 1 m) satellite images it may well be more cost-efficient to use digital aerial images, which have become readily available standard products offering extensive temporal and spatial coverage. The use of images from unmanned aerial vehicles should also be investigated.

In the present study, a semi-dense (6–9 pulses per m^2) LiDAR data and low altitude (1 km) images were used. Such data acquisition leads to high spatial sampling densities and radiometric accuracy (atmospheric effects) but the costs are high, on the order of 3–4 €/ha for large projects. For practical applications, training data will be

needed from the field, which increases the costs. If absolute calibration of the spectral values of the images could be carried out, this would reduce the need for field samples (Honkavaara 2008). In addition, a priori information on the target area, e.g. knowledge of the stand treatment history and site conditions would likely enhance the RS results. Integration of the a priori information will require further research and method development.

Acknowledgements

The authors are grateful to the Academy of Finland, Suomen Luonnonvarain Tutkimussäätiö and Metsämiesten säätiö for financing this work. We acknowledge the support by the personnel at Hyytiälä Forest Station.

References

Ahokas, E., Kaasalainen, S., Hyyppä, J. & Suomalainen, J. 2006. Calibration of the Optech ALTM 3100 laser scanner intensity data using brightness targets. International Archives of Photogrammetry, Remote Sensing and Spatial Information Sciences, 36(A1). CD-ROM. 6 p.

Axelsson, P. 2000. DEM generation from laser scanner data using TIN models. The International Archives of the Photogrammetry and Remote Sensing, Amsterdam, The Netherlands, Vol. XXXIII, Part B4/1. p. 110–117.

Cohen, J. 1960. A coefficient of agreement for nominal scales. Educational and Psychological Measurement 20(1): 37–46.

Elfving, B. 1982. Hugin´s ungskogsinventering 1976–1979. SLU, Projekt HUGIN. Rapport 27. (In Swedish).

Haddow, K.A., King D.J., Pouliot D.A., Pitt D.G. & Bell, F.W. 2000. Early regeneration conifer identification and competition cover assessment using airborne digital camera imagery. Forestry Chronicle 76(6): 11–24.

Häkli, P. 2004. Practical test on accuracy and usability of Virtual Reference Station method in Finland. FIG Working Week 2004, The Olympic Spirit in Surveying, 22–27 May, Athens, Greece. Conference Proceedings. 16 p.

Hall, R.J. & Aldred, A.H. 1992. Forest regeneration appraisal with largescale aerial photographs. Forestry Chronicle 68: 142–150.

Häme, T. 1991. Spectral interpretation of changes in forest using satellite scanner images. Acta Forestalia Fennica 222. 111 p.

— , Heiler, I. & Miguel-Ayanz, J.S. 1998. An unsupervised change detection and recognition system for forestry. International Journal of Remote Sensing 19(6): 1079–1099.

Hirschmugl, M., Ofner, M., Raggam, J. & Schardt, M. 2007. Single tree detection in very high resolution remote sensing data. Remote Sensing of Environment 110(4): 533–544.

Honkavaara, E. 2008. Calibrating digital photogrammetric airborne imaging systems using a test field. Publications of the Finnish Geodetic Institute 140. ISBN 978-951-711-275-8, ISSN 0085-6932. 60 p.

Hotanen, J.-P., Korpela, L., Mikkola, K., Mäkipää, R., Nousiainen, H., Reinikainen, A., Salemaa, M., Silfverberg, K., Tamminen, M., Tonteri, T. & Vanha-Majamaa, I. 2000. Metsä- ja suokasvien yleisyys ja runsaus 1951–1995. In: Reinikainen, A., Mäkipää, R., Vanha-Majamaa, I. & Hotanen, J.-P. (eds.). Kasvit muuttuvassa metsäluonnossa. Kustannusosakeyhtiö Tammi. ISBN 951-31-1963-7. p. 84–301. (In Finnish).

Huuskonen, S. & Hynynen, J. 2006. Timing and intensity of precommercial thinning and their effects on the first commercial thinning in Scots pine stands. Silva Fennica 40(4): 645–662.

Isenburg, M., Liu, Y., Shewchuk, J. & Snoeyink, J. 2006. Streaming computation of Delaunay triangulations. Proceedings of SIGGRAPH'06, July 2006. p. 1049–1056.

Kaasalainen, S., Hyyppä, J., Litkey, P., Hyyppä, H., Ahokas, E., Kukko, A. & Kaartinen, H. 2007. Radiometric calibration of ALS intensity. International Archives of Photogrammetry, Remote Sensing and Spatial Information Sciences 36, Part 3/W52: 201–205.

Karjalainen, E. 2006. The visual preferences for forest regeneration and field afforestation – four case studies in Finland. University of Helsinki, Faculty of Biosciences. Dissertationes Forestales 31. 111 p. http://www.metla.fi/dissertationes/df31.htm.

Korpela, I. 2006. Geometrically accurate time series

of archived aerial images and airborne lidar data in a forest environment. Silva Fennica 40(1): 109–126.

— 2008. Mapping of understory lichens with airborne discrete-return LiDAR data. Remote Sensing of Environment. 112(10): 3891–3897.

— & Välimäki, E. 2007. Talousmetsän maanpintamallinnus arkistoilmakuvista ja laserkeilauksella. Maanmittaus 82(2): 5–27. [Terrain modelling in forest conditions using archived aerial images and laser scanning]. (In Finnish).

— , Tuomola, T. & Välimäki, E. 2007. Mapping forest plots: an efficient method combining photogrammetry and field triangulation. Silva Fennica 41(3): 457–469.

Larsen, M. 2007. Single tree species classification with a hypothetical multi-spectral satellite. Remote Sensing of Environment 110(4): 523–532

Leberl, F. & Gruber M. 2005. ULTRACAM-D: Understanding some Noteworthy Capabilities. Photogrammetric week 2005. Universty of Stuttgart. Institute of Photogrammetry. http://www.ifp.uni-stuttgart.de/publications/phowo05/090leberl.pdf.

Maltamo, M., Malinen, J., Packalen, P., Suvanto, A. & Kangas, J. 2006. Nonparametric estimation of stem volume using airborne laser scanning, aerial photography, and stand-register data. Canadian Journal of Forest Research 36(2): 426–436.

Markelin, L., Ahokas, E., Honkavaara, E., Kukko, A. & Peltoniemi, J. 2005. Radiometric quality comparison of UltraCamD and analog camera. Proceedings of ISPRS Hannover Workshop 2005, "High-Resolution Earth Imaging for Geospatial Information". CD-ROM. 6 p. http://www.ipi.uni-hannover.de/fileadmin/institut/pdf/099-markelin.pdf

Miina, J. & Saksa, T. 2008. Predicting establishment of tree seedlings for evaluating methods of regeneration for Pinus sylvestris. Scandinavian Journal of Forest Research 23(1): 12–27.

Närhi, M., Maltamo, M., Packalén, P., Peltola, H. & Soimasuo, J. 2008. Kuusen taimikoiden inventointi ja taimikonhoidon kiireellisyyden määrittäminen laserkeilauksen ja metsäsuunnitelmatietojen avulla. Metsätieteen aikakauskirja 1/2008: 5–15. (In Finnish).

Næsset, E. 2004. Effects of different flying altitudes on biophysical stand properties estimated from canopy height and density measured with a small-footprint airborne scanning laser. Remote Sensing of Environment 91: 243–255.

— & Bjerknes, K.-O. 2001. Estimating tree heights and number of stems in young forest stands using airborne laser scanner data. Remote Sensing of Environment 78: 328–340.

Olofsson, K., Wallerman, J., Holmgren, J. & Olsson, H. 2006. Tree species discrimination using Z/I DMC imagery and template matching of single trees. Scandinavian Journal of Forest Research 21(7): 106–110.

Pesonen, A., Korhonen, K.T., Tuominen, S., Maltamo, M. & Lukkarinen, E. 2007. Taimikonhoitotarpeen arviointi valtakunnan metsien inventoinnin metsävarakartan pohjalta. Metsätieteen aikakauskirja 2/2007: 77–86. (In Finnish).

Piri, T. 2003. Early development of root rot in young Norway spruce planted on sites infected by Heterobasidion in southern Finland. Canadian Journal of Forest Research 33(4): 604–611.

Pitt, D.G. & Glover, G.R. 1993. Large-scale 35-mm aerial photographs for assessment of vegetation-management research plots in Eastern Canada. Canadian Journal of Forest Research 23: 2159–2169.

— , Runesson, U. & Bell, F.W. 2000. Application of large- and medium-scale aerial photographs for forest vegetation management: a case study. Forestry Chronicle 76: 903–913.

Pouliot, D.A. & King, D.J. 2005. Approaches for optimal automated individual tree crown detection in young regenerating coniferous forests. Canadian Journal of Remote Sensing 31: 256–267.

— , King, D.J., Bell, F.W. & Pitt, D.G. 2002. Automated tree crown detection and delineation in high-resolution digital camera imagery of coniferous forest regeneration. Remote Sensing of Environment 82(2–3): 322–334

— , King, D.J. & Pitt, D.G. 2005. Development and evaluation of an automated tree detection–delineation algorithm for monitoring regeneration coniferous forests. Canadian Journal of Forest Research 35: 2332–2345.

— , King, D.J. & Pitt, D.G. 2006. Automated assessment of hardwood and shrub competition in regenerating forests using leaf-off airborne imagery. Remote Sensing of Environment 102(3–4): 223–236.

Saksa, T., Uuttera, J., Kolström, T., Lehikoinen, M., Pekkarinen, A. & Sarvi, V. 2003. Clear-cut detection in boreal forest aided by remote sensing. Scandinavian Journal of Forest Research 18: 537–546.

Suvanto, A., Maltamo, M., Packalén, P. & Kangas, J. 2005. Kuviokohtaisten puustotunnusten ennustaminen laserkeilauksella. Metsätieteen aikakauskirja 4/2005: 413–428. (In Finnish).

Varjo, J. 1997. Change detection and controlling forest information using multi-temporal Landsat imagery. Acta Forestalia Fennica 258. 64 p.

Wanninger, L. 2005. Introduction to Network RTK. IAG Working Group 4.5.1: Network RTK. Available at: http://www.network-rtk.info/intro/introduction.html.

Total of 41 references